Progress In Electromagnetics Research M, Vol. 107, 1–12, 2022

Numerical Simulation and Application of Response Characteristics of High-Frequency Dielectric Logging Instrument

Chen Li[1, 2], Shaogui Deng[1, *], Zhiqiang Li[2], Yiren Fan[1], Jingjing Zhang[2], and Jutao Yang[2]

Abstract—Complex reservoirs such as fresh-water formations and water-flooded reservoirs developed by water injection have complex electrical characteristics owing to the influence of formation water salinity. It is difficult to accurately evaluate and identify the fluid in such complex reservoirs by using the conventional resistivity method. However, the water salinity of the formation has a reduced effect on its dielectric constant; therefore, dielectric logging technology can be used to effectively identify freshwater formation and evaluate the water-flooding level of the water-flooded layer. The accuracy of the formation response inversion charts of dielectric logging instruments is important for accurately evaluating fluids in complex reservoirs when these instruments are used. This study proposes a full-wave simulation method based on Maxwell's equations and the engineering parameters value of the dielectric logging instrument. The formation response conversion charts of the dielectric logging instrument are accurately calculated and can be used in practical logging; the simulation results are compared with those obtained using an equivalent magnetic dipole model. Based on the accurate simulation of the formation response of the dielectric logging instrument, a high-frequency dielectric logging instrument is developed, and it is applied to the fresh-water formation and water-flooded layer in the Nanyang and Ordos Basins.

1. INTRODUCTION

Since the 1970s, studies have investigated the application of dielectric logging technology for oil exploration [1, 2]. Schlumberger (USA) has developed various dielectric logging instruments, including a deep propagation instrument with a working frequency of 25 MHz and an electromagnetic propagation instrument with a working frequency of 1.1 GHz. Further, Halliburton (USA) has launched a high-frequency dielectric logging instrument with one generator and three receivers, and a working frequency of 1 GHz [3]. However, these early dielectric instruments had single polarization and asymmetrically arranged measurement antenna; therefore, the anisotropy of the formation could not be detected, and it was greatly affected by the well environment. Daqing Logging Company (China) developed a dielectric logging instrument with a working frequency of 60 MHz [4]. However, owing to constraints such as the accuracy of the high-frequency signal amplification acquisition measurement channel and formation inversion chart as well as the borehole environment, the measurement accuracy of the instrument and quality of the logging curve were generally poor. The low-frequency (250 kHz to 2 MHz) electromagnetic wave logging instruments developed by Schlumberger, Halliburton, etc. can measure and evaluate a formation during drilling in real time [5–8]; however, their working frequency is low, and their measured information mainly reflects the formation conductivity. Therefore, in 2008, Schlumberger launched their latest multi-frequency dielectric scanner [9]. Further, in 2011, Halliburton launched an advanced

Received 16 November 2021, Accepted 21 December 2021, Scheduled 28 December 2021

* Corresponding author: Shaogui Deng (Dengshaogui2021@126.com).

[1] School of Geosciences, China University of Petroleum (East China), Changjiangxi Road 66, Qingdao 266580, China. [2] China Research Institute of Radiowave Propagation, Jianshedong Road 84, Xinxiang 453000, China.

1 GHz high-frequency dielectric logging instrument [10]; however, they have not yet published accurate response characteristics for this instrument.

In recent years, researchers have performed numerous theoretical simulations and laboratory tests of dielectric logging instruments. Accordingly, they have investigated the relationship between the properties of the rock and the high-frequency electromagnetic wave propagation characteristics [11–13]. In 2003, Liu and Sato used the finite difference time domain method to numerically simulate the electromagnetic response of formations with different thicknesses and multiple frequencies and built a dielectric logging instrument based on a vector network analyzer [14]. In 2002, Kang et al. performed theoretical and experimental studies of dielectric logging inversion [15]; however, they did not accurately simulate the response of the dielectric logging instrument or carry out a practical logging application.

In this light, the present study proposes a full-wave simulation method based on Maxwell's equations and engineering parameters including the dielectric logging instrument framework, antenna geometry, and characteristics of the loading material. A 1 : 1 simulation model of a cross-polarized high-frequency array dielectric logging instrument is established, and the formation response diagram of dielectric logging is accurately simulated; then the developed dielectric logging instrument (Fig. 1) is applied to actual oilfield exploration in the Nanyang and Ordos Basins.

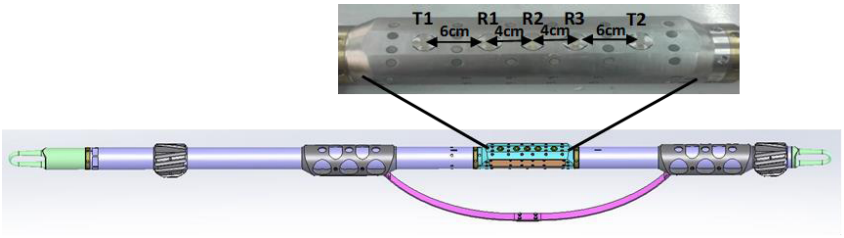

Figure 1. High-frequency array dielectric logging instrument (Mode: SHAD-1000).

2. THEORY

The basic principle of a dielectric logging instrument is as follows: an electromagnetic wave with a working frequency of 1 GHz is transmitted to the formation around the well-bore through the transmitting antenna. As this wave interacts with the formation fluid and minerals in the formation propagation process, its amplitude and phase change, and its value has a corresponding response relationship with the electromagnetic wave frequency, formation dielectric constant, conductivity, and transmission distance. By using an accurate simulation transformation chart for the formation response of the dielectric logging instrument, the dielectric constant and conductivity of the formation can be determined by amplitude attenuation and phase shift of high frequency electromagnetic wave, and then the water porosity can be determined [16].

The magnetic dipole model is usually used for electromagnetic calculations in simulations of dielectric logging instruments [17–19]; this approach uses a magnetic dipole that is equivalent to the transmitting receiving antenna, without considering the influence of the engineering parameters of the instrument, such as the antenna size, filling material, and instrument framework. Thus, the problem of the formation response characteristics of a high-frequency dielectric logging instrument is simplified to the problem of the electromagnetic field of a magnetic dipole in a multilayered medium. Although the formation conversion chart obtained using the magnetic dipole model reflects the response of the dielectric instrument under different formation conditions, the simulation results contain some errors because the influence of the engineering parameters of the instrument is not considered.

The finite integral technique was first proposed by Weiland in 1976, and it has since been used as a general scheme for spatial discretization and for calculations of various electromagnetic field problems. The full-wave simulation method based on Maxwell's equations discretizes Maxwell's equations in the integral form by using the finite integral method [20–23]. The calculation model is divided into many small grids, and the corresponding Maxwell equations are discretized into grid equations based on each grid. No approximation is used in this process (as shown in Fig. 2). The only change from the original

field equation to the grid equation is to replace the electromagnetic field quantity with its line integral or area fraction to accurately calculate the electromagnetic field.

Maxwell's integral equations		Discrete Maxwell equations
$\oint_L \vec{E}\cdot d\vec{l} = -\frac{\partial}{\partial t}\iint_S \vec{B}\cdot d\vec{S}$		$Ce = -\dot{b}$
$\oint_L \vec{H}\cdot d\vec{l} = \iint_S \left(\frac{\partial \vec{D}}{\partial T}+\vec{J}\right)\cdot d\vec{S}$	Discretization ⟹	$\tilde{C}h = j + \dot{d}$
$\oiint_S \vec{B}\cdot d\vec{s} = 0$		$Sb = 0$
$\oiint_S \vec{D}\cdot d\vec{s} = Q$		$\tilde{S}d = q$

(1)

where $\vec{E}$ is the electric field intensity (unit: V/M), $\vec{H}$ the magnetic field intensity (unit: A/M), $\vec{B}$ the magnetic induction intensity (unit: T) [3], and $\vec{d}$ the electric flux density (unit: C/m^2) [5]. C and $\tilde{C}$ are respectively discrete and adjoint discrete curl operators; the topology of the operator is only related to the structure and boundary, and their elements only include 0, 1, and -1. S and $\tilde{S}$ are respectively discrete and adjoint discrete divergence operators that represent the topological information of the structure; their elements only include 0, 1, and -1. e is the voltage of the edges of the discrete grid, b the magnetic flux on the discrete grid surface, d the electrical flux on the discrete grid surface, and h the magnetic field intensity of the edges of the discrete grid.

Compared with other numerical algorithms for solving the electromagnetic field, the main advantage of finite integration is that the continuity of the original electromagnetic field is discretized into its matrix equation; analytical field characteristics are retained; accurate electromagnetic simulation results are obtained.

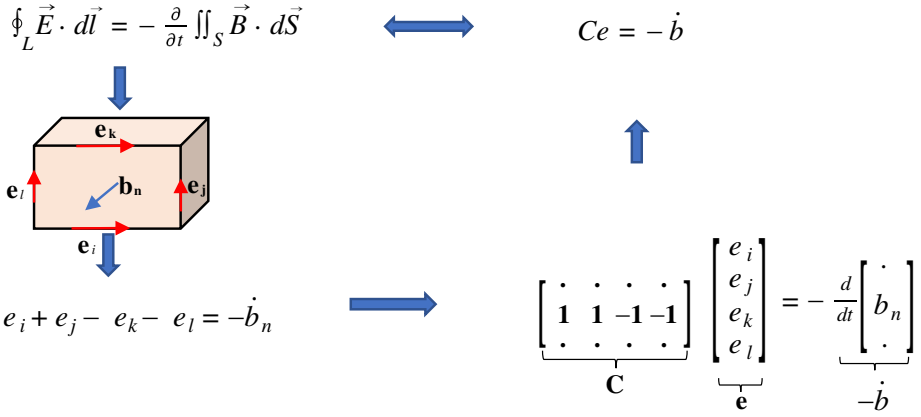

Figure 2. Discretization of Maxwell's integral equations.

3. ACCURATE SIMULATION OF DIELECTRIC LOGGING INSTRUMENT RESPONSE

3.1. Establish 1 : 1 Simulation Calculation Model of Dielectric Logging Instrument

To accurately measure the formation information using dielectric instruments, the accuracy of the formation conversion chart is very important. Therefore, the full-wave solution method with Maxwell's equations is used, and various engineering parameters such as the size, material, and instrument framework are imported to establish a 1 : 1 simulation model of the cross-polarized high-frequency array dielectric logging instrument (as shown in Fig. 3).

The dielectric logging instrument (Mode: SHAD-1000) has an inclined bow attached to the borehole wall, and the integration includes horizontal and vertical two dual-polarization transmitting antennas T1 and T2 installed on both sides and horizontal and vertical three dual-polarization receiving antennas R1, R2, and R3 installed in the middle (as shown in Fig. 3). The space between these antennas is 6-4-4-6 cm, as shown in Fig. 3. In addition, the symmetrical complementary measurement method is adopted to decrease the influence of errors in the borehole and signal amplification acquisition measurement channel. The actual operating parameters of the dielectric measuring instrument (as shown in Fig. 3) are as follows: maximum temperature of 150°C and maximum working pressure of 100 MPa. Table 1 lists the engineering parameters of the dielectric instrument.

Table 1. Engineering parameters of dielectric instrument.

Engineering parameters	Characteristic	Illustration
Maximum outside diameter of instrument	12.7 cm	Fit the size of conventional exploration well holes in an oilfield
Irregular geometry of instrument probe	Triangular surface and inlaid wear-resistant block	Effectively fit the well wall, reduce the influence of mud in the oil well, and resist wear
Material of instrument framework	1. Stainless steel model: 5Cr17Ni4Cu4N 2. Resistivity: $\rho = 88 \times 10^{-8}\,\Omega \cdot \mathrm{m}$ 3. Permeability: $\mu = 126 \times 10^{-6}\,\mathrm{H/m}$	1. High strength 2. High pressure resistance greater than 150 MPa 3. Corrosion resistance
Surface size of antenna radiation port	Length × width: 8 mm × 11 mm	1. Dual port RF signal feed 2. High pressure resistance greater than 150 MPa
Loading material of antenna	1. Material model: poly(ether-ether-ketone) 2. Dielectric constant: $\varepsilon = 3.188$ 3. Dielectric dissipation factor: $\tan\delta = 0.0046$ 4. Change in complex dielectric constant (23°–160°) $\Delta\varepsilon = \pm 0.78\%$	1. High temperature resistance (≥ 150°C) and electrical performance 2. Stable insulation performance and corrosion resistance 3. High rigidity, strength, and viscosity with metal

After the 1 : 1 simulation model of the dielectric instrument is established, and its engineering parameters are imported, the accurate formation conversion chart is calculated by the full-wave simulation method (as shown in Fig. 4).

Based on the full-wave solution method of Maxwell's equations, engineering parameters such as the instrument framework, specific size of antenna, and filling material are introduced. The formation conversion chart fluctuates irregularly at high resistivity, especially in the horizontal polarization direction.

Figure 3. Simulation model and photograph of high frequency dielectric logging instrument and antenna.

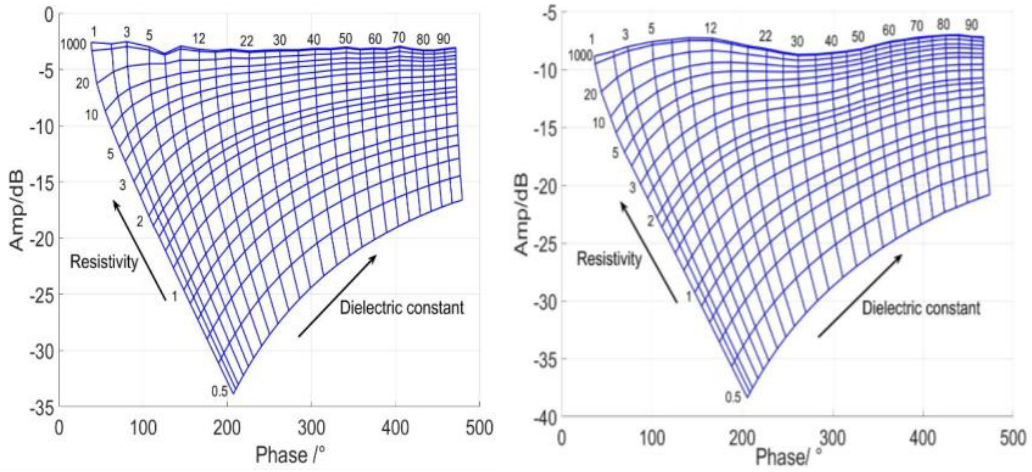

Figure 4. Stratigraphic inversion chart calculated by full-wave simulation. (a) Vertical polarization conversion chart. (b) Horizontal polarization conversion chart.

3.2. Analysis of Calculation Results

By adopting the full-wave solution method based on Maxwell's equations and introducing the abovementioned engineering parameters, the accurate formation plate of the dielectric logging instrument (indicated by the blue solid line in Fig. 5) is obtained. A comparison with the calculation results obtained using the magnetic dipole model (indicated by the red dotted line in Fig. 5) shows that the formation conversion chart accurately reflects the influence of the engineering parameters of the dielectric instrument, such as irregular fluctuations at high resistivities and overall data offset (as shown in Figs. 5(a) and (b)). The accurate and detailed stratigraphic conversion chart is in line with the application of dielectric instruments in oilfield exploration and actual logging.

To further compare the accuracy of the conversion plate of dielectric instrument simulated by the two methods, an experimental test is carried out (as shown in Fig. 6(b)). The antenna probe of the dielectric instrument is immersed in the mixed sample solution to measure its dielectric constant (as shown in Fig. 6(a)). The sample liquor includes distilled water ($\varepsilon = 80$), alcohol ($\varepsilon = 20$), and mineral

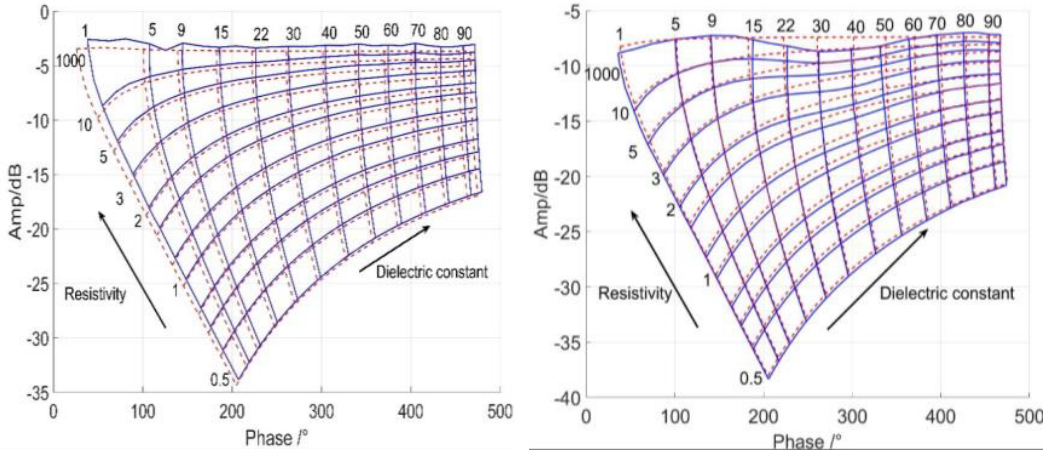

Figure 5. Comparison between accurate solution and stratigraphic inversion plate based on magnetic dipole model. (a) Comparison of vertical polarization conversion plates. (b) Comparison of horizontal polarization conversion plates.

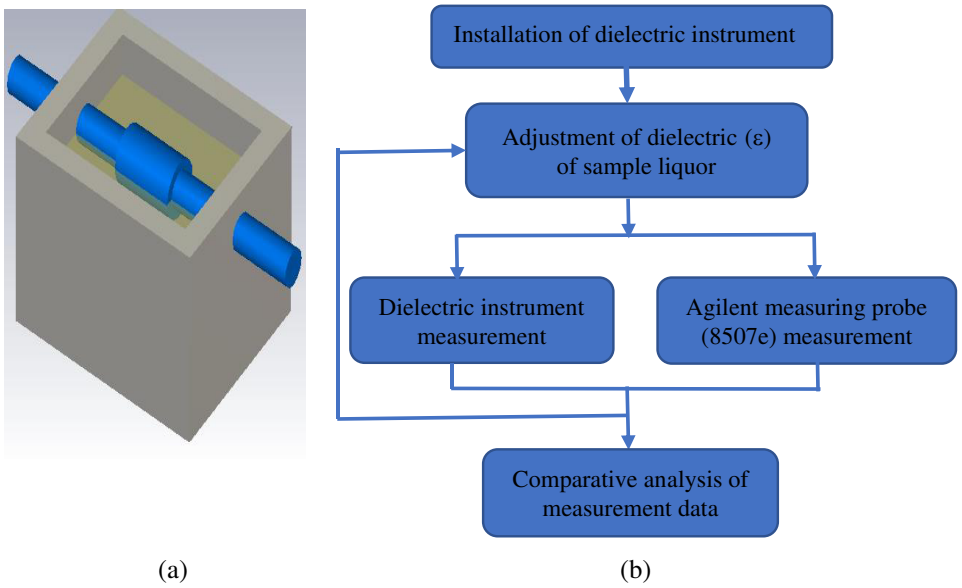

Figure 6. Schematic diagram and flow chart of dielectric instrument measurement. (a) Schematic diagram of measurement. (b) Measurement flow chart.

salt, which are mixed according to different ratios.

The test sample solution box is 80 cm long, 50 cm wide, and 30 cm high (as shown in Fig. 7(a)). In order to eliminate the electromagnetic reflection wave of the scale metal box, an absorbing material that strongly absorbs and weakly reflects the electromagnetic wave is pasted on the inner wall of the box. The dielectric constant of the sample liquor is measured with Agilent technology's dielectric measuring probe model 8507e (as shown in Fig. 7(b)).

We compared the error between the dielectric constant value inversed by the horizontal polarization plate simulated by the two models (as shown in Fig. 5(a)) and the sample solution value (as shown in Table 2). The dielectric constant calculated by the full wave simulation model is closer to the measured value of the dielectric constant of the sample solution than that calculated by the dipole model.

Table 2. Comparison of test measurement data.

Dielectric constant of sample solution measured by Agilent instrument (ε)	Dielectric constant of sample solution based on full wave simulation plate inversion (ε_1)	Dielectric constant of sample solution based on dipole simulation plate inversion (ε_2)	$\varepsilon_1 - \varepsilon$	$\varepsilon_2 - \varepsilon$
20.82	20.90	21.43	0.08	0.61
25.65	25.58	26.07	−0.07	0.42
31.55	31.60	31.52	0.05	−0.03
39.67	39.61	39.25	−0.06	−0.42
45.22	45.30	44.61	0.08	−0.61
63.62	63.56	62.90	−0.06	−0.72
78.35	78.31	78.06	−0.04	−0.29

(a) (b)

Figure 7. Actual measurement diagram of dielectric instrument. (a) Measured diagram of dielectric instrument. (b) Measured diagram of Agilent dielectric probe.

4. OILFIELD LOGGING APPLICATION OF THE DIELECTRIC INSTRUMENT

High-frequency dielectric logging instrument can measure the value of formation dielectric parameters mainly in response to the water in the formation pores. It is less influenced by rock structure and formation water salinity. It can be applied to fluid analysis as well as the identification and interpretation of complex reservoirs in oil fields, such as oil-water reservoirs in low salinity or unknown fresh-water formations.

4.1. Identification of Oil and Water in Fresh-Water Formation

Oil and gas exploration in the Nanyang Oilfield in Central China began in 1970. This oilfield has undergone five stages: conventional depressurization, steam huff and puff, hot water drive test, surfactant drive pilot test, and water injection production. These have resulted in a complex groundwater system, serious reservoir flooding and many high waters cut oil wells. Both the water and oil layers have high resistivity values, making it difficult to distinguish the two by using a conventional resistivity curve. However, the dielectric constant of the water layer is high and that of the oil layer relatively low, as seen from the dielectric logging of the Nanyang Oilfield in Fig. 8.

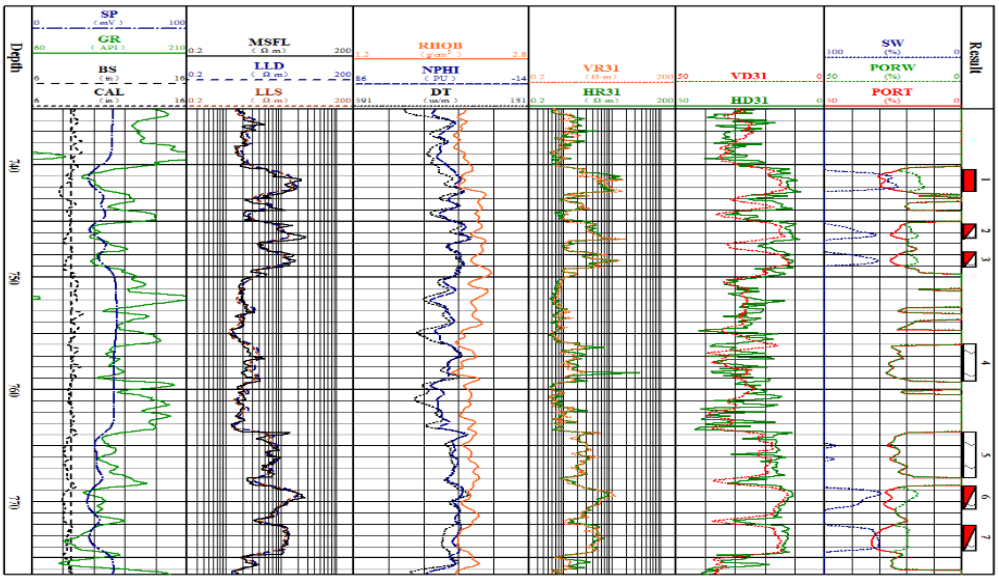

Figure 8. Results obtained by applying dielectric logging instrument to fresh-water formation.

The first column shows the well depth curve with 730–780 m. The second column shows a conventional gamma logging curve (GR) that can be applied to lithology classification to supply the formation shale content; the SP curve, a spontaneous potential logging curve; the CAL curve, a well diameter curve that reflects wellbore features; and the BS curve that indicates the bit diameter. The third column shows the LLD and LLS curves presenting the formation resistivity value measured using the dual laterolog instrument [25]. The resistivity of layers 1–6 covers one order of magnitude, ranging from 8 to 20 $\Omega \cdot$ m. Therefore, from the conventional resistivity curve measured using the dual laterolog instrument, it is difficult to make a distinction between the water and oil layers. The fourth column shows RHOB the density parameter logging curve; NPHI the neutron logging curve; and DT the acoustic logging curve that has information about the formation total porosity. The fifth column shows the VR31 and HR31 curves; these are the resistivity values in the vertical and horizontal orthogonal polarization directions of the formation, respectively, as measured with the dielectric instrument. The sixth column shows the VD31 and HD31 curves; these are dielectric parameter curves in the formation's vertical and horizontal orthogonal polarization directions, respectively, as measured with the dielectric instrument. The dielectric constant of an oil-water layer (2, 3, 6, 7) and water layer (4, 5) is higher than that of a pure oil layer (1), and in stratum (1–7), the dielectric constant of the water layer (4, 5) is maximized. In the seventh column, SW and PORW are respectively the formation water salinity and waterbearing porosity determined according to the dielectric constant logging curve. Further, the solid red line represents the total formation porosity (PORT) determined from the intersection of the neutron density in the fourth column. Because the formation's oil-bearing porosity is the difference between PORT and PORW, the formation can be finely evaluated by comparing the PORT and PORW values in the seventh column [25] as shown in Table 3.

When being applied to the Nanyang Oilfield, the dielectric logging instrument can conveniently and effectively make a distinction between the water and oil layers, thereby providing useful information for increasing the productivity of this oilfield.

4.2. Grade Evaluation of Waterflooded Layer

Since the 1980s, many oilfields in the Ordos Basin have been developed through water injection. They are presently characterized by heterogeneous large-scale water flooding and low recovery. Water injection in the low-permeability water-flooded layer has significantly changed the physical parameters of the reservoir. In particular, fresh-water flooding of the oilfield has resulted in complex changes in the resistivity with water saturation, making it difficult to evaluate the water flooding level by using a

Table 3. Results interpreted by applying dielectric logging instrument to fresh-water formation.

Layer in seventh column	Data analysis	Formation evaluation
Layer 1	HD31 = 12.5, PORT = 29.1%, PORW = 15.7%, PORW < PORT	Oil layer
Layer 2	HD31 = 12.2, PORT = 26%, PORW = 16.8%, PORW < PORT	Oil-water layer
Layer 3	HD31 = 12.5, PORT = 30.1%, PORW = 16%, PORW < PORT	Oil-water layer
Layer 4	HD31 = 27, PORT = PORW = 30%	Water layer
Layer 5	HD31 = 17, PORT = PORW = 28%	Water layer
Layer 6	HD31 = 11.5, PORT = 30.8%, PORW = 18%, PORW < PORT	Oil-water layer
Layer 7	HD31 = 12.5, PORT = 32.8%, PORW = 20%, PORW < PORT	Oil-water layer

conventional resistivity logging method [24]. Then, the dielectric constant can be used to effectively and conveniently distinguish the oil and water layers and then evaluate the water-flooding level of the water-flooded layer. Fig. 9 shows the results interpreted by applying the dielectric logging instrument to the Nanyang Oilfield.

The first curve shows the two formation curves with the same well depths of 1880–1890 m and 1920–1950 m. The second column shows that a conventional gamma logging curve (GR) can be applied to lithology classification to supply the formation shale content; the SP curve, a spontaneous potential logging curve; the CAL curve, a well diameter curve that reflects wellbore features; and the BS curve that indicates the bit diameter. The third column shows the LLD and LLS curves presenting the formation resistivity value supplied using the dual laterolog instrument. It cannot conveniently and directly evaluate the water-flooding level of the reservoir by using the resistivity curves measured with the dual laterolog instrument. In the fourth column, DEN is the density parameter logging curve, and AC is the acoustic logging curve that provides information about the formation total porosity [25]. The fifth column shows the HR31 and HR32 curves; these are the resistivity values in the formation's horizontal polarization directions, respectively, as measured with receiving antenna 3 and receiving antennas 1 and 2 of the dielectric instrument. Similarly, the sixth column shows the VR31 and VR32 curves; these are the resistivity curves in the vertical polarization direction of the formation. The seventh column shows the HD31 and HD32 curves; these are the dielectric constant in the horizontal direction of the formation as determined with the dielectric instrument. Similarly, the eighth column shows the VD31 and VD32 curves; these are the dielectric constants in the vertical direction of the formation. According to the formation dielectric constant determined using the dielectric logging instrument, the medium water-bearing flooded layer (30) is higher than that of the dielectric constant of the pure oil layer (18), and that of the heavy water-flooded layer (31, 32) is higher than that of the water-flooded layer (30). In the ninth column, SW and PORW are respectively the formation water salinity and water bearing porosity calculated using the dielectric constant logging curve. Further, the solid red line represents the total formation porosity (PORT) computed from the intersection of the neutron density. The oil-bearing porosity is defined as the difference between PORT and PORW. The oil-bearing pores of layer 18 are significantly larger than those of layers 30, 31, and 32. The seventh dielectric constant logging curve shows that the dielectric value of layer 30 is smaller than that of layers 31 and 32 but is higher than that of the upper layer 18. Therefore, it is concluded that layer 30 is a medium water-flooded layer, and layers 31 and 32 are water-flooded layers.

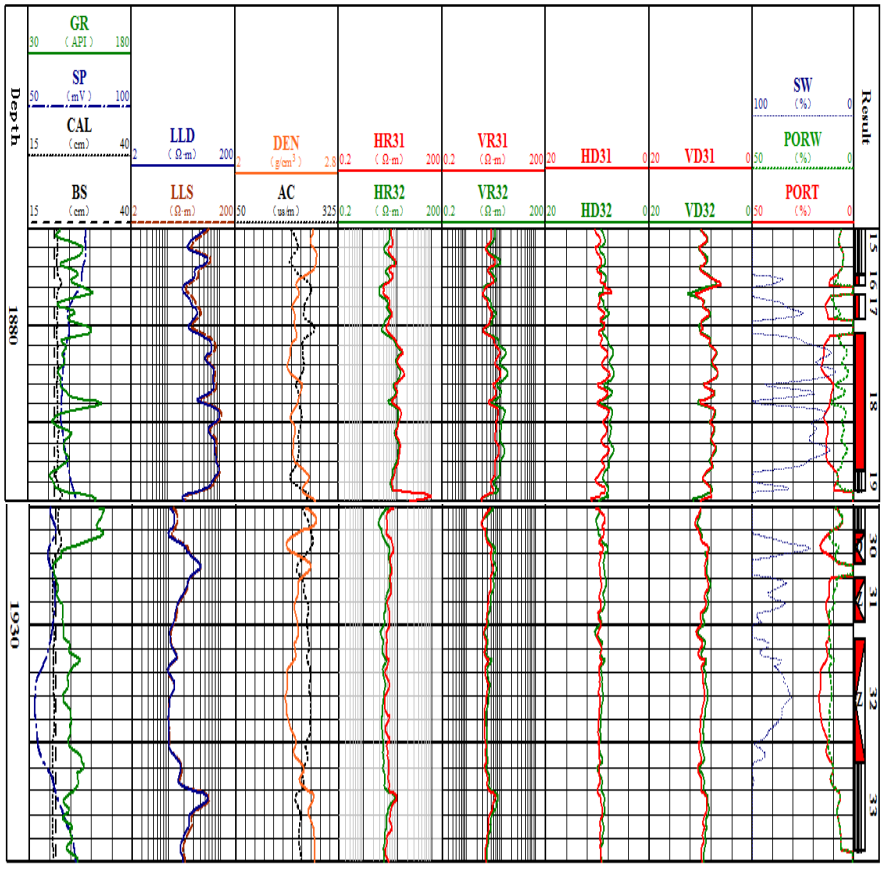

Figure 9. Results obtained by applying dielectric logging instrument to water-flooded formation.

5. CONCLUSION

By using the full-wave simulation method and engineering parameters value of a dielectric logging instrument, the formation response characteristics of a high frequency dielectric logging instrument were accurately simulated, and the formation conversion diagram of a practical dielectric logging instrument was accurately obtained. In particular, this diagram was more accurate than the one simulated using the dipole model. The practical application of the dielectric logging instrument in the Nanyang and Ordos Basins revealed that the oil-water layer in the fresh-water layer and water-flooding level of the water-flooded layer could be effectively identified and evaluated. Because these results are only obtained for the Nanyang Oilfield and Ordos Basin, the practical applicability of the dielectric logging instruments has not been sufficiently demonstrated. However, these results can be used as a reference for accurate and convenient oil-water identification and water flooding level evaluation for the middle and later development of oilfields.

ACKNOWLEDGMENT

This work was supported by the National Natural Science Foundation of China (Grant No. 42074134) and the Major Science and Technology Project of CNPC (Grant No. ZD2019184001) and Special project of national key R & D plan (2019YFC0605101).

REFERENCES

1. Freedman, R. and J. P. Vogiatzis, "Theory of microwave dielectric constant logging using the electromagnetic wave propagation method," *Geophysics*, Vol. 44, No. 5, 969–986, 1979.
2. Blenkinsop, M., P. Baker, C. Clavier, W. Kenyon, and S. des Listerine, "Deep electromagnetic propagation tool interpretation," *SPWLA 27th Annual Logging Symposium*, SPWLA-1986-XX, June 9–13, 1986.
3. Rau, R., R. Davies, M. Finke, and M. Manning, "Advance in high frequency dielectric logging," *SPWLA 32nd Annual Logging Symposium*, SPWLA-1991-S, June 16–19, 1991.
4. Song, Y. L., G. H. Chen, and M. C. Chang, "Study and application of electromagnetic logging in Daqing oilfield," *Petroleum Geological Development in Daqing*, Vol. 16, No. 4, 1997.
5. Clark, B., M. G. Liiling, J. Jundt, M. Ross, and D. Best, "A dual depth resistivity measurement for FEWD," *SPWLA 29th Annual Logging Symposium*, SPWLA-1988-A, June 5–8, 1988.
6. Clark, B., D. F. Allen, D. L. Best, et al., "Electromagnetic propagation logging while drilling: Theory and experiment," *SPE Formation Evaluation*, Vol. 5, No. 3, 263–271, SPE-18117-PA, 1990.
7. Coope, D., L. C. Shen, and F. S. C. Huang, "The theory of 2 MHz resistivity tool and its application to measurement-while-drilling," *The Log Analyst*, Vol. 25, No. 3, 1–11, 1984.
8. Yang, J., D. Omeragic, and C. B. Liu, "Bed-boundary effect removal to aid formation resistivity interpretation from LWD propagation measurements at all dip angles," *SPWLA 46th Annual Logging Symposium*, SPWLA-2005-F, 2005.
9. Schlumberger Technology Corp., "New technology and application of dielectric logging," *New technology of Oilfield*, Vol. 23, No. 1, 2011.
10. Halliburton Company, "LOGIQ high-frequency dielectric tool manual," 2011.
11. Norbisrath, J. H., "Statoil (aka Equinor), Dielectric permeability logging," *SPWLA 59th Annual Logging Symposium*, SPWLA-2018-J, June 2–6, 2018.
12. Bondarenko, A., V. Dorovsky, Yu. Perepechko, and N. Velker, "Dielectric permittivity dispersion measurements in downhole conditions — Effect on porosity measurements," *SPE Russian Petroleum Technology Conference*, SPE-176603-MS, Moscow, Russia, October 26–28, 2015.
13. Xing, G., H. Wang, and Z. Ding, "Adaptive dual-parameter deconvolution for high-frequency electromagnetic-wave logging," *IEEE Transactions on Geoscience and Remote Sensing*, Vol. 48, No. 12, 4178–4183, 2010.
14. Liu, S. X. and M. T. Y. K. Sato, "Numerical and experimental study on multi-frequency electromagnetic well logging," *Well Logging Technology*, 278–282, 2003.
15. Kang, G. J., D. B. Fang, and S. F. Zhao, "Experiment method and technique physical modeling of multi-frequent electromagnetic logging," *Journal of Jilin University (Earth Science Edition)*, Vol. 32, No. 4, 382–385, 2002.
16. Ph. Poley, J., J. J. Nooteboom, and P. J. de Waal, "Use of VHF dielectric measurements for borehole formation analysis," *Log Analyst*, Vol. 19, No. 3, 8–30, 1978.
17. Glinskikh, V. N., M. N. Nikitenko, and M. I. Epov, "Processing high-frequency electromagnetic logs from conducting formations: Linearized 2D forward and inverse solutions with regard to eddy currents," *Russian Geology and Geophysics*, Vol. 54, 1515–1521, 2013.
18. Chew, W. C., "Modeling of the dielectric logging tool at high frequencies: Theory," *IEEE Transactions on Geoscience and Remote Sensing*, Vol. 26, No. 4, 382–387, 1988.
19. Dunn, J. M., "Lateral wave propagation in a three-layered medium," *Radio Science*, Vol. 21, 787–796, 1986.
20. Weilan, T., "Time domain electromagnetic field computation with finite difference methods," *International Journal of Numerical Modeling: Electronic Networks, Devices and Fields*, Vol. 9, 293–319, 1996.
21. Graves, R., "Simulating seismic wave propagation in 3D elastic media using staggered-grid finite differences," *Bulletin of the Seismological Society of America*, Vol. 86, No. 4, 1091–1106, 1996.

22. Hirtenfelder, F., T. Lopetegi, M. Sorolla, and L. Sassi, "Designing components containing photonic bandgap structures using time domain field solvers," *Microwave Engineering*, 23–29, 2002.
23. Chieslar, J. D., "A meshing technique for large scale modeling of solution mines in salt and potash," *The 55th US Rock Mechanics/Geomechanics Symposium*, Houston, Texas, USA, June 20–23, 2021.
24. Guo, H., H. Zhang, and G. Li, "Prediction of water saturation for tight sandstone reservoirs by using array dielectric logging ADL," *The SPE Gas & Oil Technology Showcase and Conference*, Dubai, UAE, October 21–23, 2019.
25. Li, C., S. Deng, Z. Li, Y. Fan, J. Zhang, and J. Yang, "Application of high-frequency dielectric logging technology for shale oil production," *Progress in Electromagnetics Research Letters*, Vol. 100, 53–61, 2021.